Proceedings of the ASME 2009 International Mechanical Engineering Congress & Exposition
IMECE2009
November 13-19, Lake Buena Vista, Florida, USA

IMECE2009-11288

MODELING THE TEMPERATURE-DEPENDENCE OF TERTIARY CREEP DAMAGE OF A DIRECTIONALLY SOLIDIFIED NI-BASE SUPERALLOY

Calvin M. Stewart
Department of Mechanical, Materials, & Aerospace Engineering, University of Central Florida
Orlando, FL 32816-2450
calvin.stewart@knights.ucf.edu

Erik A. Hogan
Department of Mechanical, Materials, & Aerospace Engineering, University of Central Florida
Orlando, FL 32816-2450

Ali P. Gordon
Department of Mechanical, Materials, & Aerospace Engineering, University of Central Florida
Orlando, FL 32816-2450
apgordon@mail.ucf.edu

ABSTRACT

Directionally solidified (DS) Ni-base superalloys have become a commonly used material in gas turbine components. Controlled solidification during the material manufacturing process leads to a special alignment of the grain boundaries within the material. This alignment results in different material properties dependent on the orientation of the material. When used in gas turbine applications the direction of the first principle stress experienced by a component is aligned with the enhanced grain orientation leading to enhanced impact strength, high temperature creep and fatigue resistance, and improve corrosion resistance compared to off axis orientations. Of particular importance is the creep response of these DS materials. In the current study, the classical Kachanov-Rabotnov model for tertiary creep damage is implemented in a general-purpose finite element analysis (FEA) software. Creep deformation and rupture experiments are conducted on samples from a representative DS Ni-base superalloys tested at temperatures between 649 and 982°C and two orientations (longitudinally- and transversely-oriented). The secondary creep constants are analytically determined from available experimental data in literature. The simulated annealing optimization routine is utilized to determine the tertiary creep constants. Using regression analysis the creep constants are characterized for temperature and stress-dependence. A rupture time estimation model derived from the Kachanov-Rabotnov model is then parametrically exercised and compared with available experimental data.

INTRODUCTION

Creep is defined as the time-dependent, inelastic deformation of a structural component at high temperature. Creep is temperature and stress dependent. Three distinct stages of creep are considered when examining creep strain of Ni-base superalloys. The first region, called primary creep, is due to strain-hardening where pre-existing dislocations encounter obstacles and becoming immobilized [1]. It initially occurs at a high rate but the eventual saturation of dislocation density inhibits further primary creep deformation. For Ni-base superalloys, primary creep is typically small. After this period, secondary creep is characterized by an almost constant strain rate due to a balance between strain-hardening and recovery mechanics. Increased mobility enhanced by thermal activity (temperature induced diffusion) can cause cross slip where dislocations can diffuse away from obstacles [2]. In this region, the nucleation of grain boundaries and grain boundary sliding occur. Finally, tertiary creep becomes dominant and is characterized by the rapid non-linear increase of strain rate until creep rupture. The coalescence of grain boundary voids induces microcracks. Unchecked growth of cracks coupled with a net area reduction leads to rupture.

The advent of DS superalloys has lead to major advancements in the power generation industry where components experience high load and temperature environments [3]. Directional solidification involves the casting of a material so that grain boundaries are aligned at a desired orientation. The established manufacturing process is the Bridgeman vacuum casting process, where a directional heat flow is generated via remove of the shell mould from a hot zone to a cooling zone at some prescribed rate.

The result of these casting processes is a component which exhibits enhanced strength, stiffness, and/or creep resistance in a set orientation. The creep deformation and rupture response of a material is highly dependent on the nature of the grain structure of the material. While grain boundaries parallel to the load direction impart enhanced material properties, perpendicularly oriented boundaries facilitate accelerated creep deformation and rupture.

Copyright © 2009 by ASME

Downloaded From: http://proceedings.asmedigitalcollection.asme.org/ on 08/05/2015 Terms of Use: http://www.asme.org/about-asme/terms-of-use

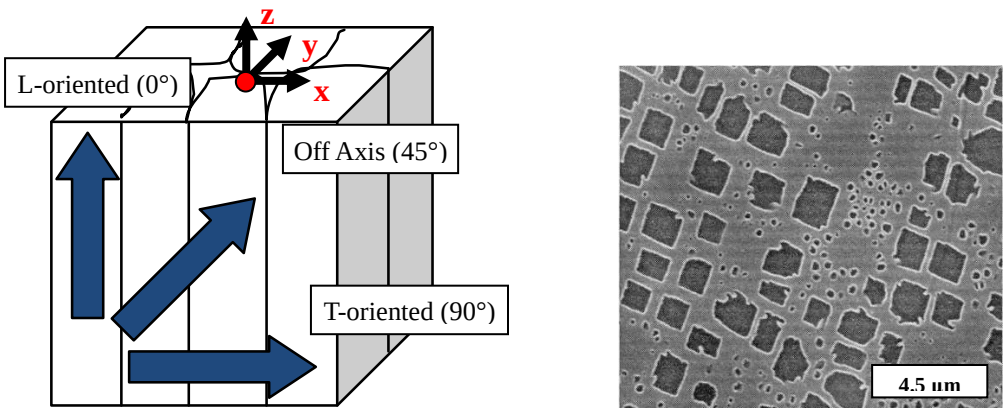

Figure 1. Structure of DS GTD-111 (a) Schematic of grain structure (b) Image of microstructure. Dark areas are the bimodally distributed γ' precipitate particles

Current industry material modeling techniques can be improved via application of more accurate constitutive models. Common practice in estimate of creep rupture life couples a secondary creep modeling with a plasticity model in numerical simulations. Secondary creep modeling alone is unable to accurately match the inelastic deformation which occurs due to the coalescence of grain boundary voids and formulation of cracks facilitating tertiary creep. This is particularly important for components under high load where the tertiary creep regime is more pronounced.

Another fault in current modeling techniques is the typical neglect of temperature dependence. This prevents the modeling of quasi-static thermal cycling and can lead to a misestimate of the creep strain as the structure experiences variable thermal loading.

In this paper, a tertiary creep damage model has been implemented to improve the prediction of creep deformation and rupture of directionally solidified components under nominally uniaxial conditions. Secondary creep constants are analytically determined based on experiments from literature [4]. A creep rupture time model is derived and utilized to determine initial tertiary creep constants. Creep deformation and rupture experiments are used in conjunction with an advanced optimization routine to determine the optimal tertiary constants at each orientation and multiple temperatures. The secondary and tertiary creep constants are written into temperature and stress dependent forms. A parametric study is carried out to determine the estimated rupture time of a DS GTD-111 specimen under a range of temperature and stress conditions.

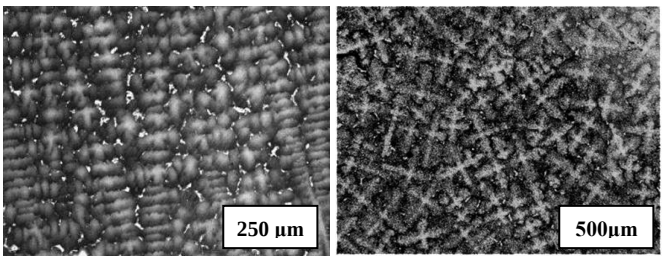

Figure 2. Grain structure of DS GTD-111 (a) T-oriented specimen (b) L-oriented specimen

MATERIAL

The material under consideration is DS GTD-111, a directionally-solidified (DS) Ni-base superalloy commonly used in gas turbine blading. Directional solidification is a technique by which the grain structure of the material can be aligned in a particular orientation. This produces a material that has enhanced stiffness, strength, and creep rupture properties in one or more local coordinate directions.

Superalloy DS GTD-111 was developed in the 1980's and is a modification of the GE superalloy Rene' 80 [5]. It is a transversely isotropic material where solidification occurs in the longitudinal (L) orientation while the two transverse (T) orientations, are uncontrolled as depicted in Figure 1a. Microstructurally, DS GTD-111 is formed of a nickel austenite (γ) matrix, bimodal gamma prime (γ') precipitated particles, γ – γ' eutectic, carbides and small amounts of topological close-packed phases σ, δ, η and laves [6],[7]. The matrix and (γ') precipitated particles are observed in Figure 1b. It has a high volume fraction of gamma prime (γ') precipitated particles, (>60%) which impart enhanced impact strength, high temperature creep and fatigue resistance, and improve corrosion resistance. This microstructure causes difficulties when considering component repair but a number of methods are under investigation to mitigate this problem[5],[8].

Due to the elongated grains the creep strain rate is dependent on orientation. Microstructural images are provided in Figure 2. In the T orientation, long grain boundaries are observed which facilitate reduced strength. The L orientation clearly shows densely packed grains which will produce enhanced strength.

Creep deformation and rupture tests were performed on L and T-oriented specimen [6]. A parametric study including temperatures ranging from 649 to 982°C and varying stress levels was implemented to determine the creep response of the material over a wide range of conditions. A list of all creep deformation and rupture tests used is found in Table 1. The experiments required three material batches, where each batch exhibited different creep responses.

Copyright © 2009 by ASME

Downloaded From: http://proceedings.asmedigitalcollection.asme.org/ on 08/05/2015 Terms of Use: http://www.asme.org/about-asme/terms-of-use

CONSTITUTIVE MODELING

To meet the research goals a constitutive model must be developed which can account for a number of conditions. In the current case, the development of primary creep is negligible. The first step is selection of a formulation which can account for steady-state secondary creep. The Norton Power law for creep, a first order differential equation for the creep strain rate is used

$$\dot{\varepsilon}_{cr} = \frac{d\varepsilon_{cr}}{dt} = A\bar{\sigma}^n \tag{1}$$

where A and n are the creep strain coefficient and exponent and $\bar{\sigma}$ is the Von Mises effective stress. Temperature-dependence is introduced in the A and n constants via an Arrhenius and polynomial function, respectively.

To account for tertiary creep a continuum damage mechanics model was applied. This involves the use of a damage variable which accounts for microstructural evolution. The damage variable is applied in a first-order differential equation for the damage evolution and coupled with the creep strain rate. Work by Kachanov [9] and Rabotnov [10] led to the coupled Kachanov-Rabotnov equations of creep

$$\dot{\varepsilon}_{cr} = \frac{d\varepsilon_{cr}}{dt} = A\left(\frac{\bar{\sigma}}{1-\omega}\right)^n \tag{2}$$

$$\dot{\omega} = \frac{d\omega}{dt} = \frac{M\bar{\sigma}^{\chi}}{(1-\omega)^{\phi}} \tag{3}$$

where the coefficient A and M and the exponents n, χ, and ϕ are material constants. Johnson and colleagues [11] show the importance of modeling beyond simple uniaxial tension conditions and focused on multi-axial states of stress. A model which can implement complex states of stress is necessary to accurately model gas turbine components. Tensile/compressive asymmetry and multi-axial behavior can be accounted for by using the damage evolution equation developed by Hayhurst [12]

$$\dot{\omega} = \frac{d\omega}{dt} = \frac{M\sigma_r^{\chi}}{(1-\omega)^{\phi}} \tag{4}$$

$$\sigma_r = \left\langle \alpha\sigma_1 + 3\beta\sigma_m + (1-\alpha-\beta)\bar{\sigma} \right\rangle \cdot \tag{5}$$

where the Von Mises stress, $\bar{\sigma}$ is replaced by the Hayhurst triaxial stress, σ_r. The Hayhurst triaxial stress is related to the principal stress, σ_1, hydrostatic (mean) stress, σ_m, and the von Mises effective stress, $\bar{\sigma}$, and includes two weight factors α and β. It should be noted that the triaxial stress becomes incompressible when $\alpha + 2\beta \geq 1$. Tensile/compressive asymmetry is thus in effect when $\alpha + 2\beta < 1$. Using equations (2), (4), and (5), a suitable tertiary creep damage model is resolved.

Studies have shown that the creep material constants A, n, M, χ, and ϕ can be determined at a constant temperature [13], [14]. Previous research shows that by determining the material constants at multiple temperatures for a material, a function can be developed, introducing temperature-dependence to the tertiary creep damage model [15]. This has the effect of making the creep strain rate and damage evolution equations temperature dependent. As temperature changes over time, the material constants change, altering the creep strain rate and

Table 1 - Creep Deformation Data and Least Square Values for DS GTD-111

	Orientation	Temperature		Stress		Primary Creep Strain	Rupture Strain	Rupture Time	Least Squares Value
		(°C)	(°F)	MPa	Ksi	(%)	(%)	(hr)	
1	L	649	1200	896	130	0.13	4.9	465.9	2.0588
2	L	760	1400	408	60	0.30	15.0	5624.0	9.6451
3	L	760	1400	613	89	0.24	13.2	243.6	1.6003
4	T	760	1400	517	75	0.60	6.9	375.7	9.029
5	T	760	1400	613	89	0.36	1.8	42.6	9.2964
6	L	816	1500	455	66	0.26	21.5	321.5	0.4058
7	T	816	1500	455	66	0.21	4.6	127.0	2.9972
8	L	871	1600	241	35	NA	18.8	2149.0	3.7922
9	L	871	1600	289	42	0.09	11.7	672.2	4.1546
10	T	871	1600	241	35	NA	7.6	980.2	8.3388
11	T	871	1600	289	42	NA	5.1	635.3	4.2331
12	L	940	1724	244	35	0.07	14.1	68.7	0.8296
13	T	940	1724	244	35	0.07	3.8	62.5	7.7568
14	L	982	1800	124	18	0.01	17.8	821.3	5.7186
15	L	982	1800	145	21	NA	9.1	301.7	0.6798

Copyright © 2009 by ASME

Downloaded From: http://proceedings.asmedigitalcollection.asme.org/ on 08/05/2015 Terms of Use: http://www.asme.org/about-asme/terms-of-use

damage evolution predicted at the current time step.

The damage evolution equation (4) can be used to obtain an estimate of rupture time. Integration of the equation leads to the following if the material is initially undamaged (i.e., ω_o=0.0)

$$t = \left[\left(1+\phi\right) M \sigma_r^{\chi}\right]^{-1} \left[1-\left(1-\omega\right)^{\phi+1}\right] \tag{6}$$

$$\omega(t) = 1-\left[1-\left(1+\phi\right) M \sigma_r^{\chi} t\right]^{\frac{1}{1+\phi}} \tag{7}$$

A limitation of these equations is they do not include the effects of secondary creep. Fortunately, for DS GTD-111 this effect is minimal due to a quick transition into the tertiary regime. Therefore, the rupture time equation is quite useful in determining an initial set of tertiary creep constants. Assuming $\omega(t)$ equals 1.0 at rupture time t_r, based on experimental data a set of initial guess tertiary constants can be found.

SECONDARY CREEP CONSTANTS

In order for the tertiary creep damage model to correctly predict creep deformation up to rupture, the creep material constants for DS GTD-111 need to be determined. Earlier work by Hyde shows that for creep models based of the classical Norton creep power law, simple analytical methods can be used to determine the secondary creep constants, A and n [16]. The minimum creep strain rate and the specimen stress load are put into equation (1) and a system solving algorithm is used to determine optimal A and n constants. Previously, Ibanez and colleagues determined the constants for DS GTD-111 but the results were not easily fittable into temperature-dependent form [6]. For the purposes of this research the constants were redetermined using a more advanced analytical formulation. The constants were determined at 649, 760, 816, 871, 940, and 982°C for L and T orientations. Dorn [17] suggested that temperature-dependence should take the form of an Arrhenius equation.

$$A(T) = B\,exp\left(\frac{-Q_{cr}}{RT}\right) \tag{8}$$

where Q_{cr} is the activation energy for creep deformation, R is the universal gas constants, and T is temperature in units Kelvin. The method produced a square of the Pearson product-moment correlation coefficient, R^2, of 0.9994 and 0.9762 for L and T orientations respectively. A plot of this is shown in Figure 3a and b. The n constant was set in the following linear form

$$n(T) = n_1 T + n_0 \tag{9}$$

with T being temperature in units Celsius. The method produced a square of the Pearson product-moment correlation coefficient, R^2, of 0.9981 and 0.9672 for L and T orientations respectively. A plot of this is shown in Figure 3c and d. Using these formulations temperature-dependence of secondary creep can be modeled.

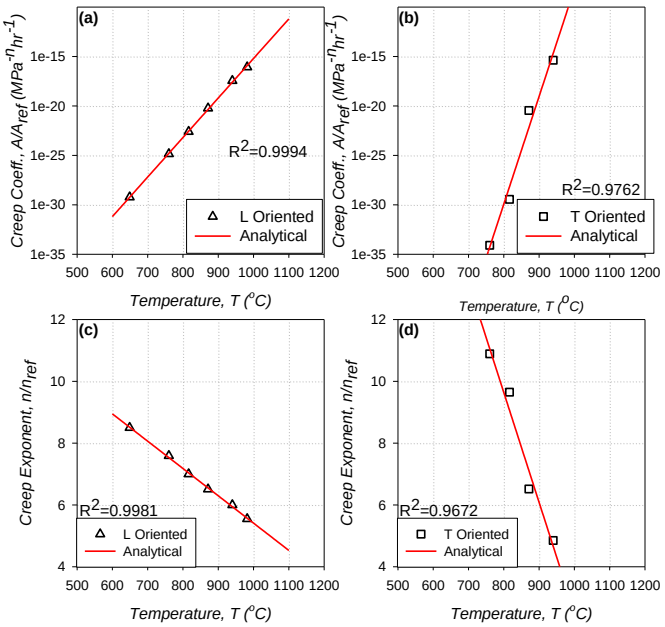

Figure 3. Secondary creep constants

NUMERICAL MODELING

The tertiary creep damage model (Eqs. (2), (4), and (5)) was implemented in a finite element analysis (FEA) software known as ANSYS. The equations were coded into a FORTRAN user-programmable feature (UPF) and compiled in the ANSYS executable. The internal state variable (ISV), ω was initialized at 0.0.

To determine the creep damage parameters M, χ, and φ, an automated optimization routine, called uSHARP, was used [18]. Finite element model (FEM) simulations were carried out and compared with their corresponding experimental data sets. In each case, the stress and temperature specified in the ANSYS simulation matched those of the corresponding experimental data set. ANSYS simulations were then executed in an iterative optimization process until the least squares values between the simulated and experimental datasets were minimized. The least squares objective function was based on creep strain, and is presented as

$$S = \frac{\sum_{i=1}^{m}\left(\varepsilon_{FEM,i} - \varepsilon_{EXP,i}\right)^2}{m} \tag{10}$$

where $\varepsilon_{FEM,i}$ and $\varepsilon_{Exp,i}$ are the strain values obtained by FEM simulation and experimental testing, respectively. The parameter m is the total number of data points resulting from an individual simulation used to determine the least squares value during a single iteration. In Eq. (10), the objective function assumes the strains correspond to an identical load time. Since the cardinality of the data sets always differed, an automated smoothing routine was carefully developed to unify time basis of the data. This feature is built into uSHARP.

Copyright © 2009 by ASME

Downloaded From: http://proceedings.asmedigitalcollection.asme.org/ on 08/05/2015 Terms of Use: http://www.asme.org/about-asme/terms-of-use

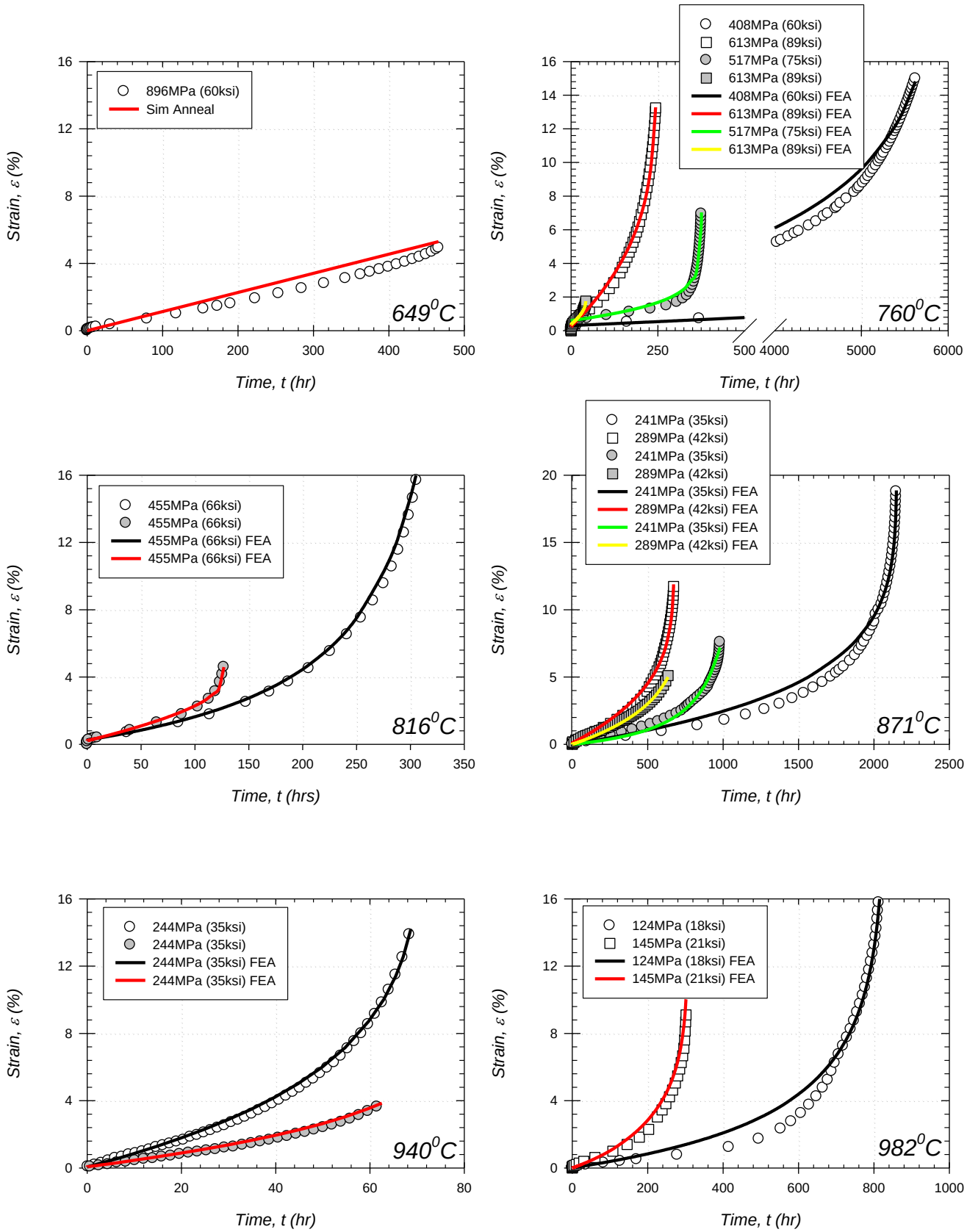

Figure 4. Creep Deformation fits of L (open) and T-oriented (shaded) DS GTD-111 at temperatures from 649-982°C

Copyright © 2009 by ASME

Downloaded From: http://proceedings.asmedigitalcollection.asme.org/ on 08/05/2015 Terms of Use: http://www.asme.org/about-asme/terms-of-use

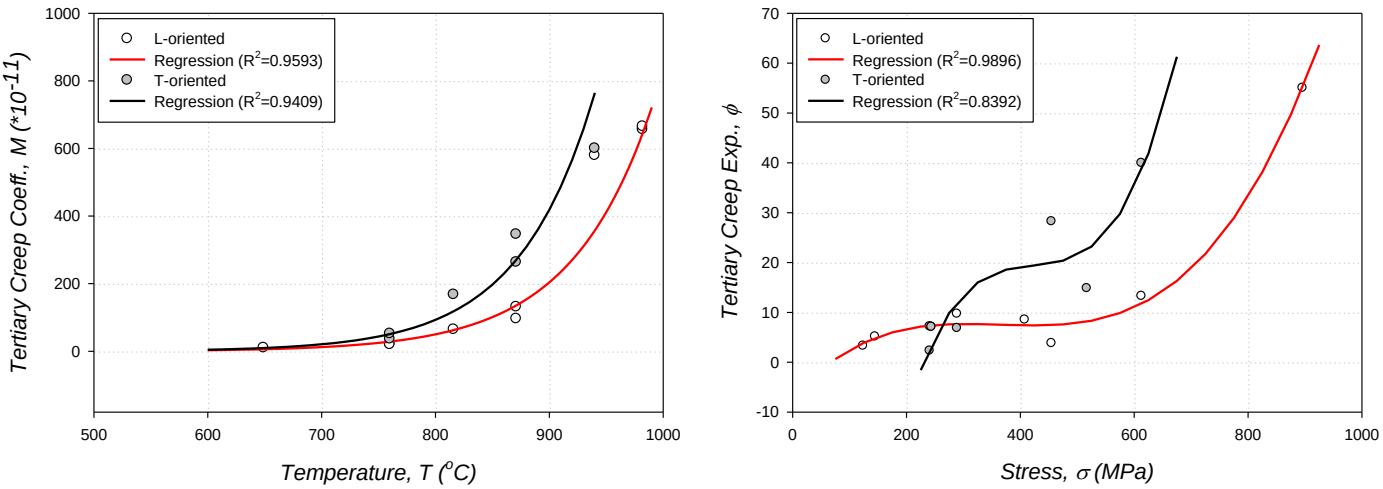

Figure 5. Temperature and stress-dependence of tertiary creep constants of DS GTD-111

The Corana et al. simulated annealing multimodal algorithm was used as the optimization algorithm [19]. It is a robust optimizer which has the capability to find the global optimal by both uphill and downhill moves. This capability allows it to effectively climb out of local minima when necessary. Additionally, its implementation into the uSHARP routine was very straightforward [20]. The uSHARP code automatically executes ANSYS at each iteration, evaluates the objective function, and updates the guess for the material constants on the basis of the simulated annealing algorithm.

Due to simulated annealing being a nonconventional algorithm it requires an extensive number of iterations before final convergence to the global optima occurs. To reduce solve time, the solve space or target range to be optimized needed to be determined. To do this, the lowest and highest temperature experiments were conducted first. The solve space was set such that the lower and upper bound for all three tertiary creep constants was $\pm 1.0 \times 10^{10}$. The results of these simulations were analyzed and target ranges for the intermediate temperature experiments was set as $0.0 \le M \le 700$, $1.7 \le \chi \le 2.3$, and $0.0 \le \phi \le 60$.

The simulated annealing routine requires an initial guess. To determine a suitable set of initial constants the derived rupture time model, equation (6), was compared with experimental data. Manual iteration of the M, χ, and ϕ was performed until the relative error between experimental and simulated rupture time was minimized. This produced constants which were readily applicable in the uSHARP routine.

For each temperature and stress condition, the optimized finite element solution has been superimposed with experimental data, as shown in Figure 4. The Kachanov-Rabotnov damage evolution equations do not account for primary creep. Therefore, primary creep strain was approximated from experimental data and added to the finite element solution. These modified creep strain values were applied in the least squares calculations and plotted with the experimental data. As a result, the secondary creep regions of each curve conferred a better fit on the tertiary creep region. This ensured that more accurate material constants were determined. The primary creep values used for each dataset are presented in Table 1.

A list of the least squares values found is in Table 1. In all cases where there was both L and T-oriented data at the same temperature and stress, the optimization routine was able to produce better least square values for the L-orientation. This is observed in Table 1 where at temperatures 760 and 816°C the L-oriented optimization improves beyond the minimum found for the T orientation.

For a number of experimental datasets, simulated annealing was unable to determine a suitable set of constants. In this experimental data, strain softening beyond the minimum creep rate is minimal. As a consequence, the creep damage parameters could not properly be optimized by uSHARP. Instead, the values for the material constants were obtained manually until a suitable set of constants could be realized. Then the least squares formulation was applied to determine the quality of fit.

TERTIARY CREEP CONSTANTS

Taking the results of the optimization routine, an automated curving fitting tool was used to determine suitable functions for the damage evolution constants. The M constant was found to work well in an exponential equation of the form

$$M(T) = \lambda_1 M_1 \, exp(\lambda_2 M_0 T)$$

$$\begin{pmatrix} \mathbf{L} \\ \mathbf{T} \end{pmatrix} orientation = \begin{cases} \lambda_1 = \lambda_2 = 1 \\ \lambda_1 = 1.2128, \lambda_2 = .93265 \end{cases} \quad (11)$$

where T is in unit Celsius and M_1 and M_0 are constants. The weight values λ_1 and λ_2, were used to implement the formulation for both L and T orientations. The ϕ and χ constants are both exponential constants within the damage evolution Eq. (4). The ϕ exponential constant produced strong correlations for stress-dependence. The ϕ exponent was found to work well in a polynomial of the form

$$\phi(\sigma) = \phi_3 \sigma^3 + \phi_2 \sigma^2 + \phi_1 \sigma + \phi_0 \quad (12)$$

Copyright © 2009 by ASME

Downloaded From: http://proceedings.asmedigitalcollection.asme.org/ on 08/05/2015 Terms of Use: http://www.asme.org/about-asme/terms-of-use

where σ is in units MPa, and ϕ_0, ϕ_1, ϕ_2, and ϕ_3 are constants (independent sets for both L and T). The fit of the temperature and stress-dependence Eqs. (11)-(12) are shown in Figure 5. The χ exponential constant is a highly sensitive constant where slight variations in value produce a large change in the resulting damage evolution. When analyzing this constant for temperature and stress-dependence independently, it was found that in a polynomial regression, temperature-dependence produced higher R^2 values of 0.4613 and 0.0236 for L and T, respectively. Unfortunately, this much variance would produce highly inaccurate results and a two-independent variable function of temperature and stress is necessary to improve correlation. The χ exponent was found to work well in a paraboloid of the form

$$\chi(T,\sigma) = \chi_0 + \chi_1 T + \chi_2 \sigma + \chi_3 T^2 + \chi_4 \sigma^2 \qquad (13)$$

where T is in unit Celsius, σ is in units MPa, and χ_0, χ_1, χ_2, χ_3, and χ_4 are constants (independent sets for both L and T). Interestingly, the L and T orientations have vastly different surface plots for the same paraboloid regression model. The regression results compared to the optimized constants are found in Table 2.

Table 2 - χ constant regression results

	Temp (C)	Stress Mpa	χ constant optimized	χ constant regressed	Error (%)
L-oriented (R^2=0.9618)	649	896	1.88	1.8904	0.55
	760	408	1.9	1.9060	0.32
	760	613	2.2314	2.2094	0.99
	816	455	2.2568	2.2273	1.31
	871	241	2.0215	1.9882	1.65
	871	289	2.054	2.1185	3.14
	940	244	2.3103	2.3465	1.57
	982	124	2.2207	2.2027	0.81
	982	145	2.2878	2.2735	0.63
T- oriented (R^2=0.8819)	760	517	2.1056	2.1097	0.19
	760	613	2.2029	2.2130	0.46
	816	455	1.981	1.9397	2.09
	871	241	2.0983	2.0521	2.20
	871	289	1.9186	2.0023	4.36
	940	244	2.2899	2.2797	0.45

All three tertiary creep constants together carry an effective accuracy measured in R^2, of 0.9593 and 0.8392 for the L and T orientations respectively. The T orientation results show more variability and overall, a lower level of correlation than that in the L orientation. This could be a symptom of the lower number of experimental tests available for the T orientation, microstructural inconsistency due to the use of three different

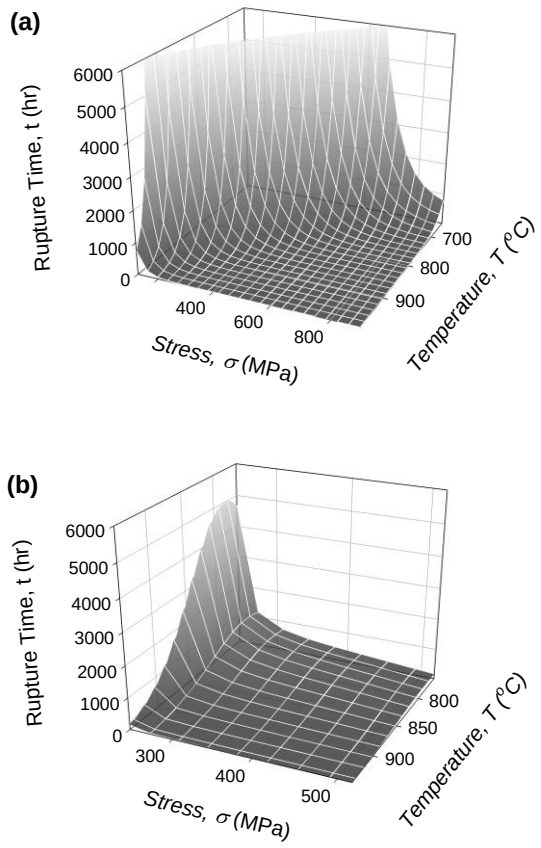

Figure 6. Parametric study using Rupture Time Model for DS GTD-111 (a) L-oriented (b) T-oriented

material batches, or could be a genuine creep property of the material in the particular orientation. Overall, the R^2 achieved could be improved by conducting additional experiments in the L and T orientations and removing outlier data points. Then a parametric regression model study could be run to determine a more optimal functional form of the χ and ϕ constants.

The implication of using these temperature-dependent functions is that it allows model structures whose boundary conditions include thermal gradients. Regions at elevated temperature will undergo a higher level of creep deformation compared to those at lower temperature. Using these functions leads to simulations that more accurately predict the locally critical points. Along similar lines, creep deformation during thermal cycling can be considered.

PARAMETRIC STUDY

Using the derived rupture time estimation model equation (6) and the temperature/stress-dependence functions for the tertiary creep constants equations (11)-(12), a tool can be generated which allows prediction of rupture time over a range of stress and thermal conditions. Using the temperature and stress ranges available from experimentation, (L oriented: 649-982°C and 125-896 MPa ; T oriented: 760-940°C and 244-517MPa), a parametric list of estimated rupture times for both L and T orientations was produce.

Copyright © 2009 by ASME

Downloaded From: http://proceedings.asmedigitalcollection.asme.org/ on 08/05/2015 Terms of Use: http://www.asme.org/about-asme/terms-of-use

Table 3 - Rupture Time Model Results

	Temp (°C)	Stress MPa	Rupture Time Model, t_r (hr) Experiments	Optimized	Regressed	% Error (relative to Exp.) Optimized	Regressed
L-oriented	649	896	465.88	502.89	777.34	7.94	66.85
	760	408	5624	5533.23	4407.98	1.61	21.62
	760	613	243.55	213.60	191.08	12.30	21.54
	816	455	321.5	326.46	226.86	1.54	29.44
	871	241	2149	1952.81	1619.19	9.13	24.65
	871	289	672.21	629.08	520.66	6.42	22.55
	940	244	68.68	65.29	83.33	4.94	21.34
	982	124	821.31	799.95	781.48	2.60	4.85
	982	145	301.68	278.66	322.04	7.63	6.75
					Average	6.0	24.4
T- oriented	760	517	375.71	338.30	157.38	9.96	58.11
	760	613	42.64	34.13	33.88	19.95	20.53
	816	455	126.96	110.79	283.33	12.74	123.17
	871	241	980.16	1158.53	1261.55	18.20	28.71
	871	289	635.33	701.93	334.24	10.48	47.39
	940	244	62.518	70.49	104.21	12.76	66.69
					Average	14.0	57.4

The results of this work can be observed in Table 3. Using the optimized constants directly, the rupture time model performs well in the L orientation and moderately in the T orientation with an error on average of 6% and 14% respectively. Implementation of the regression models reduces the accuracy of the rupture time model in both orientations. The L orientation can still be considered a valid estimate with an error on average of 24.4%. However, the T orientation due to a lower effective R^2 value found in the regression models becomes highly inaccurate at an error on average of 57.4%.

In Figure 6, mesh 3D plots of the rupture time for L and T orientations are shown. For the L orientation (Figure 6a), the rupture time model shows that rupture time is strongly codependent on stress and temperature. This co-dependence is expected due to the uniform distribution of grain boundaries observed in this orientation. In the T orientation on the other hand (Figure 6b), the material still exhibits codependence but with a stronger dependence on temperature at low stress. This could be indicative of the sliding and migration of the long grain boundaries in this orientation at high temperature.

CONCLUSIONS

The modified Kachanov-Rabotnov tertiary creep damage material model performed well in modeling the creep response of the DS GTD-111 superalloy. Utilization of the simulated annealing optimization routine produced tertiary creep constants which accurately predicted the creep deformation at various stress and temperature conditions. The later developed temperature and stress-dependent regression models were found to accurately and moderately match the optimized tertiary creep constants in the L and T orientations respectively. Application of the rupture time estimation model show that it can closely predict rupture times found in experimental data for the L and T orientation. Future work will focus on improving the quality of the T oriented temperature and stress-dependence regression formulations via additional mechanical testing.

ACKNOWLEDGEMENTS

Calvin Stewart is thankful for the support of a Mcknight Doctoral Fellowship through the Florida Education Fund.

REFERENCES

[1] Kassner, M. E. , and Pérez-Prado M., 2004, *Fundamentals of creep in metals and alloys*, Elsevier, pp.47-49.
[2] Penny, R. K., and Marriott, D. L., 1995, *Design for Creep*, Springer, pp.11.
[3] Daleo, J.A. and Wilson, J.R., 1998, "GTD111 alloy material study," Journal of Engineering for Gas Turbines and Power, Transactions of the ASME, **120**(2), pp. 375-382.
[4] Ibanez, A. R., 2003, "Modeling creep behavior in a directionally solidified nickel base superalloy," Ph.D. Dissertation, Georgia Institute of Technology, Atlanta, GA.
[5] Li, L., 2006, "Repair of directionally solidified superalloy GTD-111 by laser-engineered net shaping," Journal of Materials Science, **41**(23), pp. 7886-7893.
[6] Ibanez, A. R., Srinivasan, V. S., and Saxena, A., 2006,

Copyright © 2009 by ASME

Downloaded From: http://proceedings.asmedigitalcollection.asme.org/ on 08/05/2015 Terms of Use: http://www.asme.org/about-asme/terms-of-use

"Creep deformation and rupture behaviour of directionally solidified GTD 111 superalloy," Fatigue & Fracture of Engineering Materials & Structures, **29**(12), pp. 1010-1020.
[7] Sajjadi, S. A., and Nategh, S., 2001, "A high temperature deformation mechanism map for the high performance Ni-base superalloy GTD-111," Materials Science and Engineering A, **307**(1-2), pp. 158-164.
[8] Hale, J. M., 1994, "Procedure development for the repair of GTD-111 gas turbine bucket material," *Eighth Congress &Exposition on Gas Turbines in Cogeneration and Utility*, Portland, OR.
[9] Kachanov, L. M., 1958, "Time to Rupture Process Under Creep Conditions," Izv. Akad. Nank. (8), pp. 26-31.
[10] Rabotnov, Y. N., 1969, *Creep Problems in Structural Members*, North Holland, Amsterdam.
[11] Johnson, A. E., Henderson, J., and Khan, B., 1962, *Complex-Stress Creep, Relaxation and Fracture of Metallic Alloys*, HMSO, England. Chap. 6.
[12] Hayhurst, D. R., 1983, "On the Role of Continuum Damage on Structural Mechanics," Engineering Approaches to High Temperature Design, B. Wilshire and D. R. J. Owen, eds., Pineridge Press, Swansea, UK, pp. 85–233.
[13] Hyde, T. H., Becker, A. A., and Sun, W., 2001, "Creep Damage Analysis of Short Cracks Using Narrow Notch Specimen made from a Ni-base Superalloy at 700°C," *10th International Conference on Fracture*, Honolulu, Oahu, HI.
[14] Altenbach, J., Altenbach, H., and Naumenko, K., 2004, "Edge Effects in Moderately Think Plates under Creep-Damage Conditions," Technische Mechanik, **24**(3-4), pp. 254-263.
[15] Stewart, C. M., and Gordon, A. P., 2008, "Modeling the Temperature-dependence of Tertiary Creep Damage of a Ni-Base Alloy," ASME Early Career Technical Journal, **7**(1), pp. 1-8.
[16] Hyde, T. H., Sun, W., Tang A., 1998, "Determination of the material constants in creep continuum damage constitutive equations" Strain, **34**(3), pp. 83-90.
[17] Dorn, J.E., 1955, "Some Fundamental experiements on high temperature creep", Journal of the Mechanics and Physics of Solids, **3**.
[18] Hogan, E. A., 2009, "An efficient method for the optimization of Viscoplastic constitutive model constants," Honors in the Major Undergraduate Thesis, University of Central Florida, Orlando, FL.
[19] Corana, A., Marchesi, M., Martini, C., and Ridella, S., 1987, "Minimizing Multimodal Functions of Continuous Variables with the 'Simulated Annealing" Algorithm," ACM Transactions on Mathematical Software, **13**(3), pp. 262-280.
[20] Goffe, W. L., Gary, D. F., and Rogers, J., 1993, "Global Optimization of Statistical Functions with Simulated Annealing," Journal of Econometrics, **60**(1/2), pp. 65-100.

Copyright © 2009 by ASME

Downloaded From: http://proceedings.asmedigitalcollection.asme.org/ on 08/05/2015 Terms of Use: http://www.asme.org/about-asme/terms-of-use